

## HIGH TIME-RESOLUTION OBSERVATIONS OF THE VELA PULSAR

SIMON JOHNSTON<sup>1</sup>, WILLEM VAN STRATEN<sup>2</sup>, MICHAEL KRAMER<sup>3</sup>, AND MATTHEW BAILES<sup>2</sup>*Draft version October 31, 2018*

## ABSTRACT

We present high time resolution observations of single pulses from the Vela pulsar (PSR B0833–45) made with a baseband recording system at observing frequencies of 660 and 1413 MHz. We have discovered two startling features in the 1413 MHz single pulse data. The first is the presence of giant micro-pulses which are confined to the leading edge of the pulse profile. One of these pulses has a peak flux density in excess of 2500 Jy, more than 40 times the integrated pulse peak. The second new result is the presence of a large amplitude gaussian component on the trailing edge of the pulse profile. This component can exceed the main pulse in intensity but is switched on only relatively rarely. Fluctuation spectra reveal a possible periodicity in this feature of 140 pulse periods. Unlike the rest of the profile, this component has low net polarization and emits predominantly in the orthogonal mode. This feature appears to be unique to the Vela pulsar. We have also detected microstructure in the Vela pulsar for the first time. These same features are present in the 660 MHz data. We suggest that the full width of the Vela pulse profile might be as large as 10 ms but that the conal edges emit only rarely.

*Subject headings:* pulsars: individual (PSR B0833–45)

## 1. INTRODUCTION

The Vela pulsar is one of the closest and brightest radio pulsars known. Polarization observations made shortly after its discovery showed that it is highly linearly polarized and that the position angle of the radiation followed an S-shape curve as a function of pulse longitude (Radhakrishnan & Cooke 1969). This showed that the radio emission was related to the geometry of the magnetic field lines near the pole. The rotating vector model (RVM) of Radhakrishnan & Cooke has been extensively used in a large number of pulsars to obtain the spin axis - magnetic axis and the viewing angle - magnetic axis geometries. In the Vela pulsar, the angle between the spin and magnetic axes,  $\alpha$  is estimated to lie between  $60^\circ$  and  $90^\circ$ , and the impact angle,  $\beta$  is  $\sim -6^\circ$  (Krishnamohan & Downs 1983 (hereafter KD83); Lyne & Manchester 1988; Rankin 1993).

In the only detailed single pulse study of Vela to have appeared in the (recent) literature, KD83 observed 87000 pulses at 2.3 GHz with a time resolution including dispersion smearing of  $750\mu\text{s}$ . Their main conclusion was that the pulse profile consists of four different components which were emitted at different heights in the magnetosphere. They also found that the pulse shape depended on the intensity with the strongest pulses arriving early with respect to the average profile.

In some pulsars, the S-shaped sweep of polarization is broken by one or more jumps of  $90^\circ$ . These are known as ‘orthogonal’ jumps (Backer & Rankin 1980). It is generally believed that emission from two orthogonally polarized modes are superposed (McKinnon & Stinebring 1998). At a given pulse longitude the dominant mode then determines the position angle. In the Vela pulsar, KD83 found that only one mode was present at all pulse longitudes for all 87000 pulses.

Sub-pulse structure is ubiquitous in pulsars on a number of different timescales. So-called microstructure is often seen and can have both a typical width (generally a few tens of  $\mu\text{s}$ ) and be quasi-periodic in a given pulsar (e.g. Lange et al. 1998).

Surprisingly, for the Vela pulsar no microstructure analysis has ever been published.

The phenomenon of giant pulses has only been detected in two pulsars, the Crab pulsar (e.g. Lundgren et al. 1995) and PSR B1937+21 (Cognard et al. 1996). The working definition of giant pulses is a flux density in a single pulse which is more than 10 times the mean flux density. Both the Crab and PSR B1937+21 show occasional pulses in excess of 1000 times the mean pulsed flux. In the vast majority of pulsars, very few if any single pulse fluxes exceed 10 times the mean flux density. The Crab is one of the youngest known pulsars whereas PSR B1937+21 is a millisecond pulsar with very rapid rotation rate. As Cognard et al. (1996) point out, the common feature these pulsars share is the highest (estimated) magnetic field at their light cylinder, although whether this is related to the physics of the giant pulses is unclear. In this parameter, Vela ranks 22nd in the current catalogue of 965 pulsars.

## 2. OBSERVATIONS AND DATA REDUCTION

As part of a project investigating single pulses from a large sample of pulsars, we observed the Vela pulsar at two different observing frequencies between 2000 March 14 and 17 using the 64-m Parkes radiotelescope. The center frequencies of the observations were 660 and 1413 MHz; at these frequencies the system equivalent flux density is 120 and 26 Jy respectively. Each receiver consists of two orthogonal feeds sensitive to linear polarization. The signals are down-converted and amplified before being passed into the backend. The backend, CPSR, is an enhanced version of the Caltech Baseband Recorder (Jenet et al. 1997). It consists of an analogue dual-channel down-converter and digitizer card which yields 2-bit quadrature samples at 20 MHz. The data stream is written to DLT for subsequent off-line processing allowing all 4 Stokes parameters to be computed. At both frequencies, 30 minutes of data or  $\sim 20000$  pulses were recorded. Before each observation, a 90-s observation of a pulsed signal, directly injected into the receiver at a

<sup>1</sup>Research Centre for Theoretical Astrophysics, University of Sydney, NSW 2006, Australia

<sup>2</sup>Swinburne Centre for Astrophysics and Supercomputing, Swinburne University of Technology, Hawthorn, Vic 3122, Australia

<sup>3</sup>University of Manchester, Jodrell Bank Observatory, Macclesfield, Cheshire SK11 9DL, UK

45° angle to the feed, is made. This enables instrumental polarization to be corrected. Observations of the flux calibrator Hydra A were made at each of the observing frequencies; this allows absolute fluxes to be obtained.

The data were processed off-line using a workstation cluster at the Swinburne Supercomputer Centre. Data reduction involves coherent de-dispersion (Hankins & Rickett 1975) and includes quantization error corrections as described by Jenet & Anderson (1998). The data are folded at the apparent topocentric period of the pulsar and the full Stokes profiles for each pulse are written to disk. Flux calibration and instrumental calibration are then carried out using information contained in the observation of the pulsed (calibration) signal. The data in each frequency channel is corrected for the rotation measure of the pulsar and all the frequency channels are then summed to produce the final profile. At 1413 MHz there are 2048 time-bins per pulse period for an effective time resolution of 44  $\mu$ s, comparable to the scatter broadening at this frequency. At the lower frequency, the time resolution is 88  $\mu$ s, but the scatter broadening dominates and the effective time resolution is  $\sim 0.5$  ms at 660 MHz.

### 3. RESULTS

#### 3.1. Microstructure

As far as we are aware, the literature has not pointed out the existence of microstructure in the Vela pulsar, generally because the time resolution of the observations has been too coarse. Figure 1 shows ‘typical’ single pulses from Vela at 1413 MHz with a time resolution of 44  $\mu$ s. Microstructure is clearly seen. This microstructure is ubiquitous in virtually every pulse at 1413 MHz. We conclude that the smooth pulse profiles shown by KD83 are an artifact of their coarse time resolution.

At lower observing frequencies, pulse scatter broadening smooths over the microstructure features, although they are still visible in the 660 MHz data. A complete investigation of the microstructure in the Vela pulsar will be presented elsewhere (Kramer et al. 2001).

#### 3.2. Pulse Intensity

Figure 2 shows a histogram of the mean flux density for the 20085 pulses recorded at 1413 MHz. More than 95% of the pulses are within a factor of 2 of the mean flux density, 99.5% are within a factor of 3 and there are no pulses greater than 10 times the mean flux density. This distribution is typical of many, perhaps most pulsars. There are no giant pulses in Vela in the same sense as those in the Crab pulsar and PSR B1937+21. It is well known that Vela does not show any nulls (e.g. KD83; Biggs 1986), and indeed we also see no evidence of nulling in the  $\sim 40,000$  pulses collected at the two observing frequencies. The weakest single pulses have continuum flux densities of 1.3 and 0.3 Jy at 660 and 1413 MHz respectively.

We computed the modulation index,  $\sigma_i/m_i$  where  $\sigma_i$  is the rms and  $m_i$  the mean intensity in the  $i$ th bin, for each bin in the pulse profile. As also shown by KD83, the modulation index is low in the centre of the pulse profile and increases towards the wings. To show this effect in a more striking way, we computed the quantity  $R_i=(\text{MAX}_i-m_i)/\sigma_i$  where  $\text{MAX}_i$  is the maximum intensity in the  $i$ th bin.  $R_i$  as a function of pulse phase is shown in Figure 3. It can be seen that the value of  $R$  is consistent with Gaussian statistics in the centre of the pulse but that both the leading and trailing edges of the pulse have individual pulses

which are extremely high amplitude with respect to the mean intensity. A very similar result is seen at 660 MHz. The three main features in this plot will be discussed in more detail below.

#### 3.3. Orthogonal Modes

The sweep of the position angle across the pulse in the Vela pulsar shows the characteristic S shape without any of the ‘orthogonal’ jumps seen in a large number of other pulsars. The swing of the position angle is well fitted by the RVM and shows that the line-of-sight cuts very close to the magnetic axis, i.e.  $\alpha \sim 55^\circ$  and  $\beta \sim -6^\circ$ . To investigate whether any individual pulse shows emission in the orthogonal mode we compared the position angle of each bin in each pulse to that of the position angle in the integrated profile at the same pulse phase. Of the 40,000 pulses recorded at 660 and 1413 MHz, *none* shows evidence for orthogonal mode emission in the region of the profile’s peak, consistent with the results of KD83 at 2295 MHz.

However, investigating the feature centered near phase +4 ms in Figure 3, we discovered that it is a result of only 21 pulses at 1413 MHz. These pulses not only exhibit integrated flux densities more than 10 times that of the integrated profile at this longitude, but they also have a consistently small fractional polarization. Similarly, at 660 MHz there are 23 pulses with the same characteristics. Of these, all had low net polarization but, where polarization was present it was orthogonal to the integrated polarization at this pulse phase. Figure 4 shows the profile resulting from the summation of the 21 pulses taken at 1413 MHz. The large intensity of this ‘bump’ feature compared to the integrated profile and the orthogonal mode emission can clearly be seen. We also note that the circular polarization is negative under the bump emission and this is of the opposite sign to that in the integrated profile, as is commonly seen in orthogonal mode emission. Introducing a jump of 90° in the position angle of the bump region results in the identical results for  $\alpha$  and  $\beta$  when fitting the RVM.

The midpoint of the ‘bump’ emission occurs 3.86 ms after the main pulse peak at 1413 MHz and 4.37 ms afterwards at 660 MHz, a significant difference. Thus the profile is wider at 660 MHz than at 1413 MHz. The ‘bump’ component is also stronger relative to the main pulse at 1413 MHz than at 660 MHz by nearly a factor of 2. This frequency dependence is in the direction expected in the radius-to-frequency mapping paradigm. Such a high intensity, relatively rarely-appearing component has not been detected in any other pulsar although the interpulse in PSR B0950+08 may show similar properties.

As stated above, at 1413 MHz there are 21 occurrences of the bump component in the  $\sim 20000$  pulses. A look at the pulse numbers, however, reveals a far from random sequence. There are 7 cases in which the differences in pulse number between appearances of the bump component is less than 300. Of these, 5 pairs have intervals either in the range 130-140 pulses or 260-280 pulses and other related harmonics are also present. We computed fluctuation spectra from the single pulses, producing results which are somewhat different to those of KD83, probably due to our much better time resolution. Including 15360 pulses in our analysis, we indeed find periodicities of  $\sim 0.007$  and  $\sim 0.025$  cycles/period, i.e. every  $\sim 142$  and  $\sim 40$  pulses, in the ‘bump’ region. These periodicities are significant at the  $\gtrsim 6\sigma$  level. We also detect an even lower frequency feature in the main peak region, which could be associated with a ‘drift’ in micropulses, which we sometimes observe. A longer dataset is required to determine the significance of these features; observations at 1400 and 2400 MHz will be carried out in the near

future.

### 3.4. Giant Micro-pulses

At 1413 MHz there are 14 pulses for which  $R > 25$  and which do not occur in the bump region. The individual pulses are shown superimposed in Figure 5. Of these 14, the two which occur earliest in pulse phase are both centered at phase  $-2.2$  ms (relative to the peak of the integrated profile) and are very narrow with a full-width at half-maximum of only  $\sim 50 \mu\text{s}$ . The other 12 pulses have peak phases between  $-1.4$  and  $-1.8$  ms and have typical half-widths of  $\sim 400 \mu\text{s}$ . The brightest of these pulses has a peak flux density in excess of 2500 Jy, more than 40 times the peak flux density in the integrated profile and more than 130 times the mean flux density at this pulse phase. At 660 MHz the results are very similar. One high amplitude pulse is seen at early phases and 19 at phases just prior to the main pulse. The peak amplitudes are again in excess of 2000 Jy, this is only a factor of  $\sim 10$  higher than the peak of the main pulse at this frequency.

We call all these features giant micro-pulses : they are not true giant pulses because their mean flux density does not exceed 10 times the mean flux density, but their peak flux densities are very large in absolute terms and they appear far more often than would be expected from any ‘normal’ flux probability distribution. The polarization of these giant micro-pulses is extremely high with a linear fraction close to 100%. Furthermore, the position angle of the polarization is exactly that expected by extrapolating the main position angle swing back to these longitudes. Finally, 13 of the 14 pulses have small negative circular polarization and one has positive circular polarization.

Although KD83 also noted that strong intensity pulses arrived at early phases, they make no explicit mention of single giant pulses. However, they seem to have employed a time-averaging technique which may have had the effect of broadening the giant pulses (because they do not all arrive at the same pulse phase) and reducing their amplitude. Our secondary feature more than 2 ms earlier than the main pulse peak was not covered in their ‘on-pulse’ bins.

## 4. DISCUSSION

If we assume that the line-of-sight crosses the magnetic axis at the peak of the profile, we can compute the emission height at 660 and 1413 MHz by measuring the delay of the steepest swing of the position angle relative to the profile peak (Blaskiewicz et al. 1991; Hibschan & Arons 2000). Using the result of our RVM fits, the delay is 1.3 ms at 660 MHz and 1.04 ms at 1413 MHz leading to emission heights of 98 and 78 km respectively, although the 660 MHz value has a significant error bar due to the scatter broadening. These emission heights are typical in pulsars, and the frequency scaling is also within the range seen in other pulsars (e.g. Kramer et al. 1994). In turn, by assuming dipolar field lines, the emission heights can be used to derive the half-opening angle of the cone,

$\rho = 3\sqrt{\pi r_{em}/(2cP)}$ , respectively  $13^\circ$  and  $11.6^\circ$  at the two frequencies.

Knowledge of  $\rho$  and the viewing geometry can be used to derive the width of the pulse profile. (Normally this process is used in reverse, with the known pulse width used to derive  $\rho$ ). For  $\alpha \sim 55^\circ$  and  $\beta \sim -6^\circ$ , the pulse full-width should be  $\sim 30^\circ$  or  $\sim 7.4$  ms. Even when considering that this width is to be measured at a very low intensity level, it seems much larger than observed in the integrated profile. However, the emission from the ‘bump’ component now extends the pulse profile towards the trailing edge, matching the expected width quite nicely. Luo & Melrose (2001) have recently proposed that the trailing edges of wide cones have their emission suppressed due to cyclotron absorption within the pulsar magnetosphere. Such a mechanism may explain why these ‘bump’ pulses are seen so rarely.

The presented calculation assumes that the magnetic axis coincides with the pulse peak, tempting the speculation that we are ‘missing’ the leading edge of the cone. Perhaps extending to a phase of  $-5$  ms, the cone may not emit at all or only very rarely. We note that the giant micro-pulses do increase the pulse width on the leading edge but only by 1 ms or so.

One could also assume that, with the extra bump component, we are seeing the full pulse width. In this case, the magnetic pole crossing would be close to phase  $+2$  ms. However, this reasoning does not fit well with a number of the observations. First, the steepest swing of the position angle sweep occurs *prior* to this point. Also, the frequency dependence of the pulse width and the spectral index of the various features show that the ‘main’ pulse is more likely to be the core component and the ‘bump’ more likely to be conal (e.g. Kramer et al. 1994).

Considering the apparent two groups of giant micro-pulses, it is unclear whether we are dealing with two separate phenomenon or whether the small number statistics are preventing us from seeing these features at all pulse phases near  $-2$  ms. However, the giant micro-pulses at the earliest phases are of much shorter duration than those occurring later, and the same pattern is seen at 660 MHz as at 1413 MHz. What is certain is that they all lead the main pulse; there are no such features anywhere after the main pulse peak.

These giant micro-pulses seem to have more in common with the giant pulses in PSR B1937+21 than with the Crab giant pulses. In the former, the giant pulses all occur at the same pulse phase, whereas in the Crab the giant pulses can arrive anywhere within the pulse window. In Vela, the giant micro-pulses all arrive within a narrow phase range and lead the main pulse (unlike in PSR B1937+21 where the giant pulses lag the main pulse).

We thank R. Edwards for help with the observations. The Australia Telescope is funded by the Commonwealth of Australia for operation as a National Facility managed by the CSIRO.

## REFERENCES

- Backer, D. C. & Rankin, J. 1980, ApJ Supp. Series, 42, 143  
 Blaskiewicz, M., Cordes, J. M. & Wasserman, I. 1991, ApJ, 370, 643  
 Cognard, I., Shrauner, J. A., Taylor, J. H. & Thorsett, S. E. 1996, ApJ, L81  
 Foster, R. S. & Hankins, T. 1995, ApJ, 453, 433  
 Hankins, T. H. & Rickett, B. J. 1975, Meth. Comp. Phys., 14, 55  
 Hibschan, J. A. & Arons J., 2000, astro-ph/0008117  
 Jenet, F. A., Cook, W. R., Prince, T. A. & Unwin, S. C. 1997, PASP, 109, 707  
 Jenet, F. A. & Anderson, S. B. 1998, PASP, 110, 1467  
 Kramer, M., Johnston, S. & van Straten, W. 2001, In Preparation  
 Kramer, M., Wielebinski, R., Jessner, A., Gil, J. A., Seiradakis, J. H., 1994, A&AS, 107, 515  
 Krishnamohan, S. & Downs, G. S. 1983, ApJ, 265, 372 (KD83)  
 Lange, C., Kramer, M., Wielebinski, R. & Jessner, A. 1998, A&A, 332, 111  
 Luo, C. G., Melrose, D. M., Ulu-oguz, M. J., & Johnston, S. 2001, MNRAS, 321, 1007

FIG. 1.— Two individual pulses at 1413 MHz showing microstructure. Zero phase refers to the peak of the integrated profile.

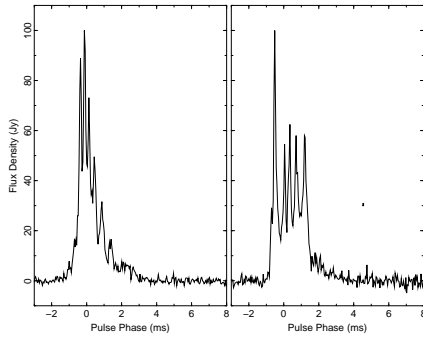


FIG. 2.— The histogram of mean flux densities observed for 20085 pulses at 1413 MHz. The flux distribution is similar to other pulsars in that very few strong pulses are seen.

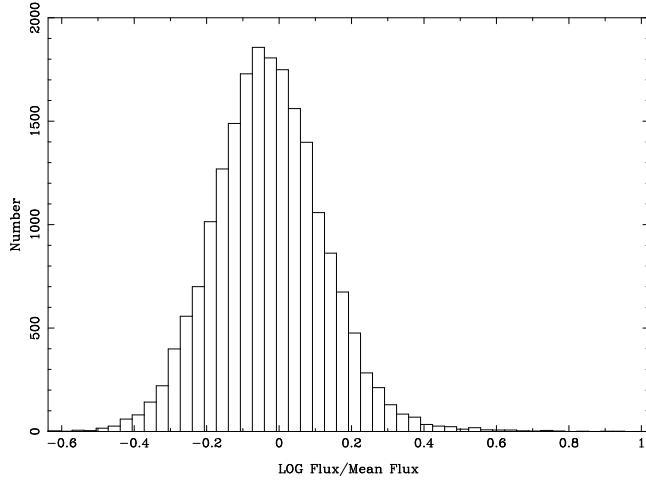


FIG. 3.— The  $R$  parameter (see text) as function of pulse longitude at 1413 MHz. Zero phase refers to the peak of the integrated profile. The horizontal solid line represents the expected value if the intensity were normally distributed.

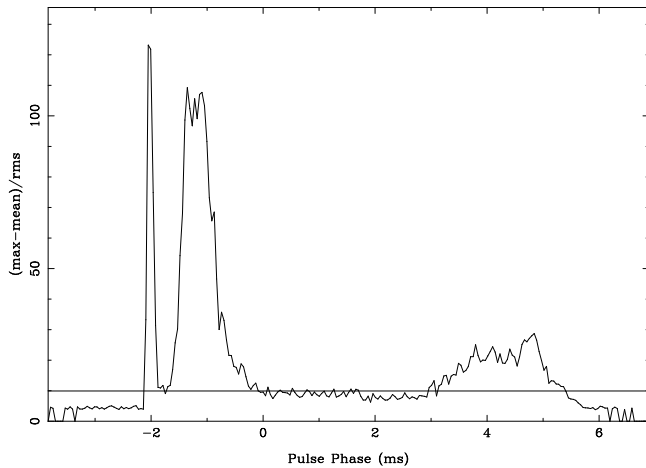


FIG. 4.— The integrated profile from 21 pulses at 1413 MHz which exhibit an additional ‘bump’ feature at the trailing part of the profile. The bump is orthogonally polarized compared to the main profile. The top panel shows the swing of position angle as a function of pulse phase. The bottom panel shows the total intensity (thick line), linear polarization (dashed line) and circular polarization (dotted line). The smooth thick line is the integrated profile from 20000 pulses using the same flux density scale.

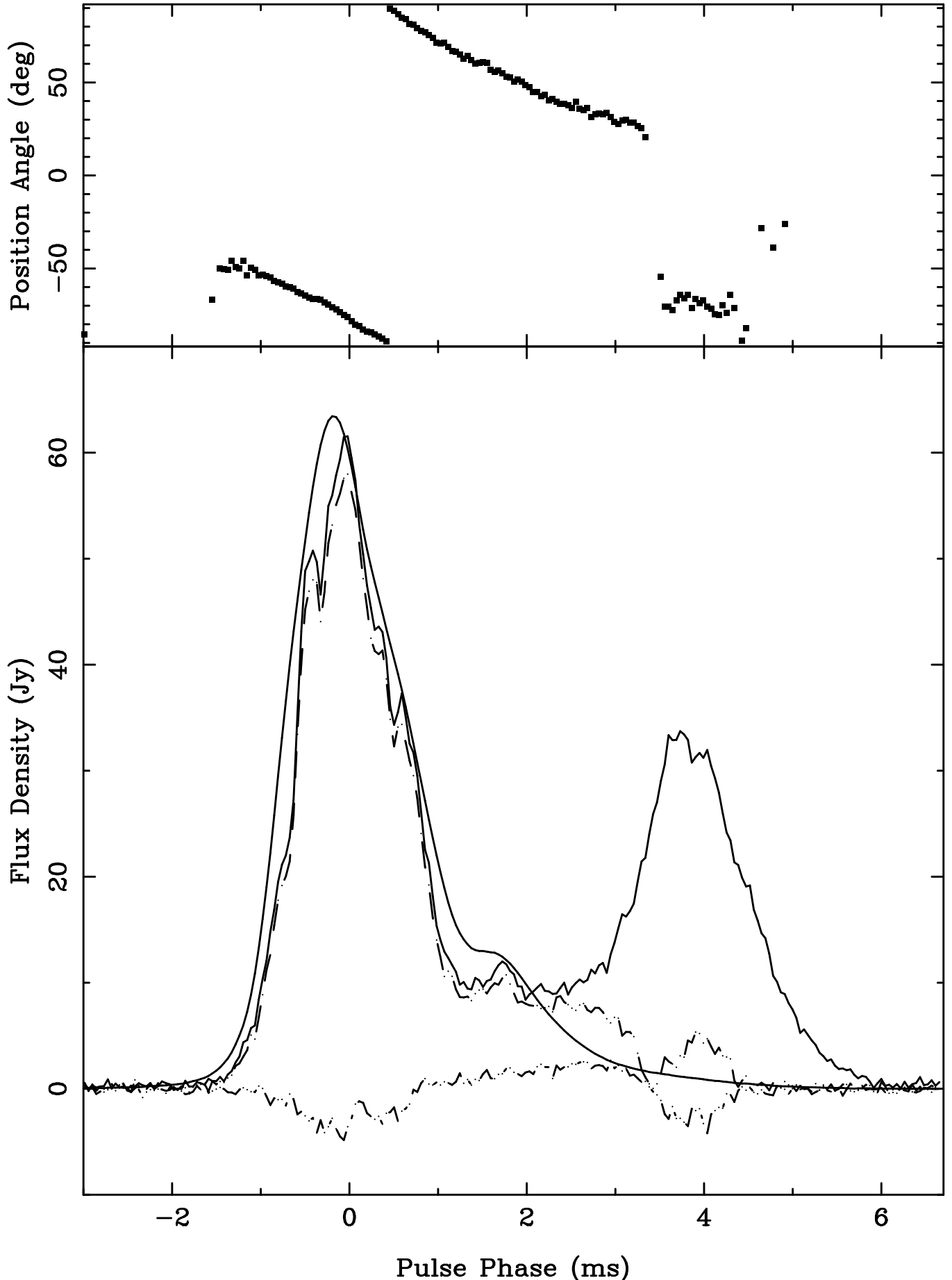


FIG. 5.— A superposition of 14 giant micro-pulses at 1413 MHz occurring at early pulse phases. Only the total intensity is shown. In comparison, the integrated profile has a peak flux of only 60 Jy.

